On the Electrical Characterization of Electroadhesive Displays and the Prominent Interfacial Gap Impedance Associated with Sliding Fingertips

Craig D. Shultz, Michael A. Peshkin, and J. Edward Colgate

***Abstract*— We report on the characterization of two variable friction electroadhesive displays using careful electrical and electrochemical impedance measurements. We qualitatively and quantitatively examine the properties of the skin, body, surface coating, and various electrode interface impedances in isolation using different contact interface conditions and measurement types. A lumped series impedance model explains how all impedances are related during normal usage, and the linearity of this model is shown to be valid under certain assumptions, such as high applied frequencies or small applied currents. Speculation as to the physical mechanisms underlying each impedance element is also given. This analysis unambiguously verifies the existence of a previously hypothesized key electrical system parameter: the sliding interfacial impedance (or air gap impedance). This parameter represents the large increase (100-1000 percent) in overall electrical impedance observed when a finger is sliding versus when it is stationary. It is concluded that this impedance increase cannot be explained by other measured electrical impedance elements in the system and that it vanishes again when the finger comes to rest.**

I. Introduction and Background

Observations of electroadhesion, or the increased attraction between two contacting surfaces caused by an electric field applied across their interface, have been recorded for over 140 years. Throughout the late 19th and 20th centuries the effect intrigued scientists and engineers, causing tactile vibrations and sounds to be emitted via their fingertips, almost as if by magic [1] [2] [3] [4]. Modern day application of this effect, however, has so far been limited. It has been used for semiconductor wafer chucking [5], for industrial material handling and robotic gripping [6] [7], as a tactile display technology for the visually impaired [8] [9], and, most recently, as a visuo-tactile display technology for general tablet and smartphone type interactions [10] [11].

It is this last application that has garnered renewed interest in electroadhesion, specifically as it pertains to the development of high performance variable friction surface haptic devices [12] [13]. With this interest comes the need for effective modeling techniques that are tailored to the specific application of fingertip adhesion, and metrics for creating optimized skin based electroadhesive systems. To date, a variety of groups have used perceptual and/or force measurements to characterize displays, as this is usually the output that is ultimately desired from the interaction [11] [14] [15] [16] [17]. Typically, a voltage is input to the electroadhesive system, and the resulting force or perception output is measured, with an approximate theoretical model linking the two. While essential for evaluating the capabilities of existing hardware, this black box type approach is limited in terms of designing new electroadhesive systems. It lacks empirical measurements of electrical parameters for the systems in question, and usually relies heavily on values pulled from the literature to roughly map applied voltage input to recorded force and perceptual output.

In this work, we propose an alternate approach, and carry out a set of electrical characterization techniques to examine two electroadhesive surfaces (one common to the literature, and one relatively new) and experimentally look inside the black box. We asked these two questions: what factors affect how an applied voltage (or current) results in an effective interfacial voltage in the system, and how does this interfacial voltage translate into an additional lateral force on the finger? The latter is addressed in a separate work [13], while former is investigated here.

To answer this first question, we developed a model inspired by the semiconductor chuck literature [18] and previous surface haptic research [19], which uses parameters taken almost entirely from empirical measurement. We then validate this model with I versus V Lissajous curve observations and use small signal electrical and electrochemical impedance measurements to capture model parameters. Finally, we discuss how isolated measurements and those taken as a whole converge to unambiguously confirm the existence of a prominent interfacial gap impedance. Finally, we show how this gap impedance compares to other elements in the system.

II. Materials and Methods

A. Apparatus and Surfaces

The tribometer and amplifier setup introduced in [13] is used here. It is built around a velocity controlled turntable, high speed data acquisition board (DAQ), and rotating normal force sensing platform. The amplifier is a custom built current controlled amplifier which has a large signal -3dB bandwidth of 45 kHz and the ability to source or sink up to 5mA at $\pm$250 V.

The electroadhesive surfaces used were two 150 mm diameter disks, seen in Fig. 3. The first surface coating tested was cut from part of a commercial touch screen system sold by 3M under the name MicroTouch. This surface coating is widely used in the surface haptics literature [11] [14] [16] [17], which is why it was chosen here. The nominal series capacitance of these screens was bypassed by using silver epoxy to make a direct electrical connection to the transparent indium tin oxide (ITO) conductive layer. The coating itself

C D Shultz, M A Peshkin, and J E Colgate are with the Mechanical Engineering Department, Northwestern University, Evanston, IL, 60208, USA. craigdshultz {@u.northwestern.edu}, peshkin, colgate {@northwestern.edu}

is an approximately 1 μm thick layer of SiO_2. The surface roughness was measured using an optical profilometer, and was found to have an RMS roughness value of 193nm. It is referred to as the 3M coating. The second coating tested was a diamond like carbon (DLC) coating, identical to the coating in [13]. It is approximately 2μm thick, and goes by the tradename BALINIT DYLYN PRO. It was applied to an aluminum disk using a chemical vapor deposition process, has a RMS roughness of 35nm, and is referred to as the DLC coating.

B. Current and Voltage Sensing

The setup seen in Fig. 1 was used for all electrical measurements presented. The current controlled amplifier applied a test current to an unknown impedance, Z_{ut}, and actual current was measured using a series shunt resistor (1 kΩ 0.1%). This value was small with respect to most impedances measured, thus introducing negligible error. Regardless, it was subtracted from all impedance measurements.

Voltage was monitored using a custom 50:1 high impedance ($\approx 500M\Omega||10pF$) probe. This high impedance ensures that, even for unknown impedances on the order of $10M\Omega||100pF$, the majority of output current travels through the impedance under test, and is not diverted through the probe. The voltage probe and current shunt voltages were buffered by high precision op-amps (OPA192, Texas Instruments Inc., TX, USA) and sampled by the DAQ. Under these conditions, impedances ranging from $\approx 10^3 - 10^8\Omega$ may be measured with minimal error due to probing.

C. Electrode and Interface Contact Conditions

Four different electrode and interface conditions, seen Fig. 2, were used. They can be broken into a purely electrical impedance condition (I), an electrochemical bioimpedance condition (II), and two conditions that include both electrochemical and electrical impedances (III), (IV). Gross area of contact was held constant between each condition at just under 1 cm^2. The lead author's non-dominant index finger was used in conditions (II), (III), and (IV).

Condition (I) was used to investigate the properties of the 3M and DLC dielectric coatings in isolation. Current was supplied to the conductive substrate (ITO or aluminum) and was returned via a copper disc electrode. The copper electrode was coupled to the top side of the coating using a thin layer of conductive silver grease (MG Chemicals 8463). With electrodes on the top and bottom of the coating layer, the impedance through this layer could be measured.

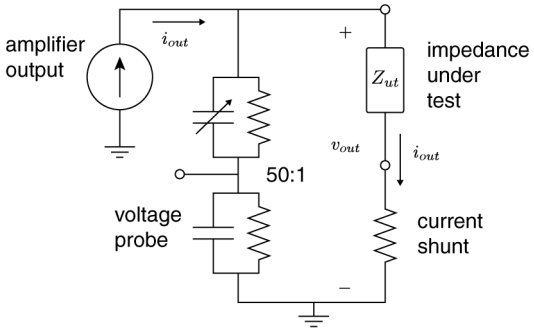

Fig. 1. Current and voltage measuring setup consisting of a 50:1 impedance divider probe and low side current shunt resistor.

Condition (II) was used to probe the bioimpedance of the skin and body. Current was supplied to the fingertip via a Ag/AgCl electrode with solid electrolyte gel filled sponge (3M Red Dot 9641), seen Fig. 4. The Ag/AgCl interface provides very low and stable DC and AC polarization impedances associated with the electronic to ionic conversion, and also has a very low half-cell potential. In addition, the solid gel electrolyte limits the wetting and penetration of the electrolyte into the skin of the finger, and allows the contact area to be approximately constant and well defined [20]. An isolated measurement of two electrodes back to back confirmed that the electrode's combined polarizing and electrolyte gel impedance was far below other measured impedances.

From the electrode, current travels through the skin of the fingertip, down the hand, and exists the body on the ventral forearm via two Ag/AgCl electrodes of the same type which had a combined 6 times larger contact area than the fingertip electrode. The impedance due to this wrist interface was measured (using a 3 electrode configuration) and found to be approximately 10 times smaller in magnitude than the impedance measured from the fingertip, meaning its bioimpedance contribution is minimal.

Interface conditions (III) and (IV) represent the total electrical impedance that is observed as a finger interacts with each electroadhesive surface. They are used to investigate aspects of electroadhesion which are directly relevant to its practical application, and which illuminate the underlying principles of operation. Current is applied to the electroadhesive surface, as in condition (I), travels through the surface coating, across the coating/skin interface, through the skin and body, and is returned via the Ag/AgCl electrodes at the wrist described in condition (II). Applied normal force was held at 1 N by the subject using feedback from the normal force platform.

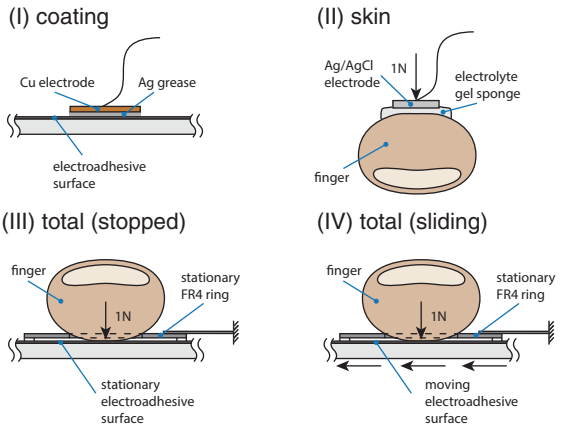

Fig. 2. Side view of 4 interface conditions: (I) the surface coating in isolation, (II) the skin in isolation, (III) the total impedance of a stationary finger on the surface, and (IV) the total impedance during sliding between the skin and coating (not to scale).

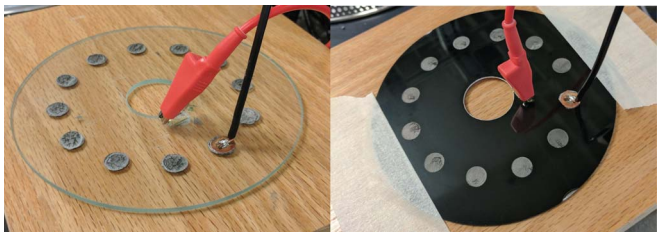

Fig. 3. The 3M coated surface (left) and DLC coated surface (right) with silver conductive grease applied at 12 different locations. These locations represent where the impedance through the coating layers was measured.

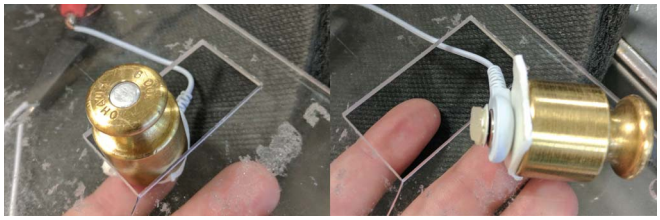

Fig. 4. Conditions at the fingertip for measuring the bioimpedance of the skin and body. The small Ag/AgCl electrode was stamped out from a larger electrode, and attached to a weight, which was then allowed to bear against the finger. An acrylic frame constrained the weight horizontally.

During condition (III), the finger and surface are stationary, while in condition (IV) the surface slides under the finger with a constant velocity of 170 mm/s. Apparent area of contact is controlled by use of a small FR4 ring, which is glued to perimeter of the skin contact patch and mechanically grounded via a carbon fiber rod. This ring is the same as the force ring in [13], but here is is only used constrain the contact area and hold the finger still while the surface slides.

III. Model and Definitions

A. Electrical Impedance Model

We adopt a series gap impedance based approach, introduced by Shultz et al. in [19]. This model assumes that the only voltage which is frictionally relevant is that which develops across the small interfacial gap between the finger and surface, called V_{gap}. Analysis of this assumption is presented else ware [13], and is not within the scope of this work. Instead, we attempt to relate the air gap voltage, V_{gap}, to more macroscopic system parameters such as total applied current, I_{total}, and voltage, V_{total}, by assuming a linear lumped series impedance model, Fig. 5, and performing measurements to investigate these impedances.

B. Definition of Skin and Coating Impedances

This model lumps the skin and body bioimpedances into a single Z_{skin}, which describes the impedance seen looking from the outside surface of the stratum corneum through the skin and body to ground. In a similar manner, we define the bulk dielectric coating impedance, $Z_{coating}$, as the impedance seen looking from the top surface of the coating through the coating itself back to the current source.

C. Definition of Total Impedance

The total impedance Z_{total}, is defined as the total observed impedance seen during normal operation from the output

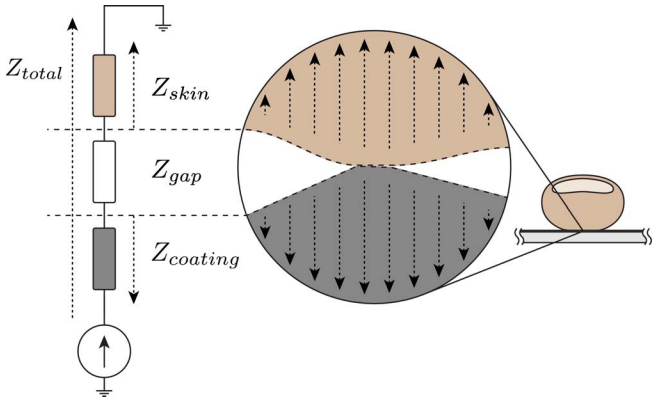

Fig. 5. Lumped series electrical impedance model (left) showing the definitions of the skin, gap, coating, and total impedance parameters. Also shown in a conceptual image of the gap (right), where the outer of the skin touches the top surface of the coating at a small asperity point. The interfacial gap consists of a small number of these asperity points, and is mostly filled with air elsewhere.

of current controlled amplifier through the electroadhesive coating, contact interface, skin, body, and to ground. It is measured under two conditions, when the surface is sliding relative to the finger, $Z_{total(sliding)}$, and when the surface and finger are stationary, $Z_{total(stopped)}$.

D. Definition of Gap Impedance

The gap impedance, Z_{gap}, is the hardest impedance to define. This is because the gap impedance is used to capture and describe the interface conditions between the skin and the coating surface. As such, it is a variable impedance that can possibly change with spatially dependent parameters such as skin/surface geometry and relative motion, as well as time dependent parameters such as sweat accumulation or viscoelasticity of the skin. For a complete description, the electrode polarization impedance associated with this interface, including the electric double layer and any Faradaic current paths, should also be theoretically included.

With this description, we see it is impossible to define the gap impedance in isolation, but rather that it should always be described with respect to Z_{total} and set of contacting surfaces and conditions. Therefore, we define the gap impedance, Z_{gap}, as the impedance that remains from a given measurement of Z_{total} after other known impedances in the system have been accounted for.

IV. I vs V Curve Experiments

A. Data Collection

The first assumption tested for in our impedance model was linearity. This was done by generating a collection of Lissajous curves to inspect the behavior of the different conditions. A sinusoidal current of $\pm 0.1mA$ was applied using interface conditions (I), (II), and (IV). Conditions (I) and (IV) were measured with both the 3M and DLC coating, each at a single representative location. Six frequencies were chosen, from 0.1 Hz to 10,000 Hz. Voltage and current were sampled at 50x the excitation frequency for 20 complete cycles. The resulting data was bandpass filtered digitally, with

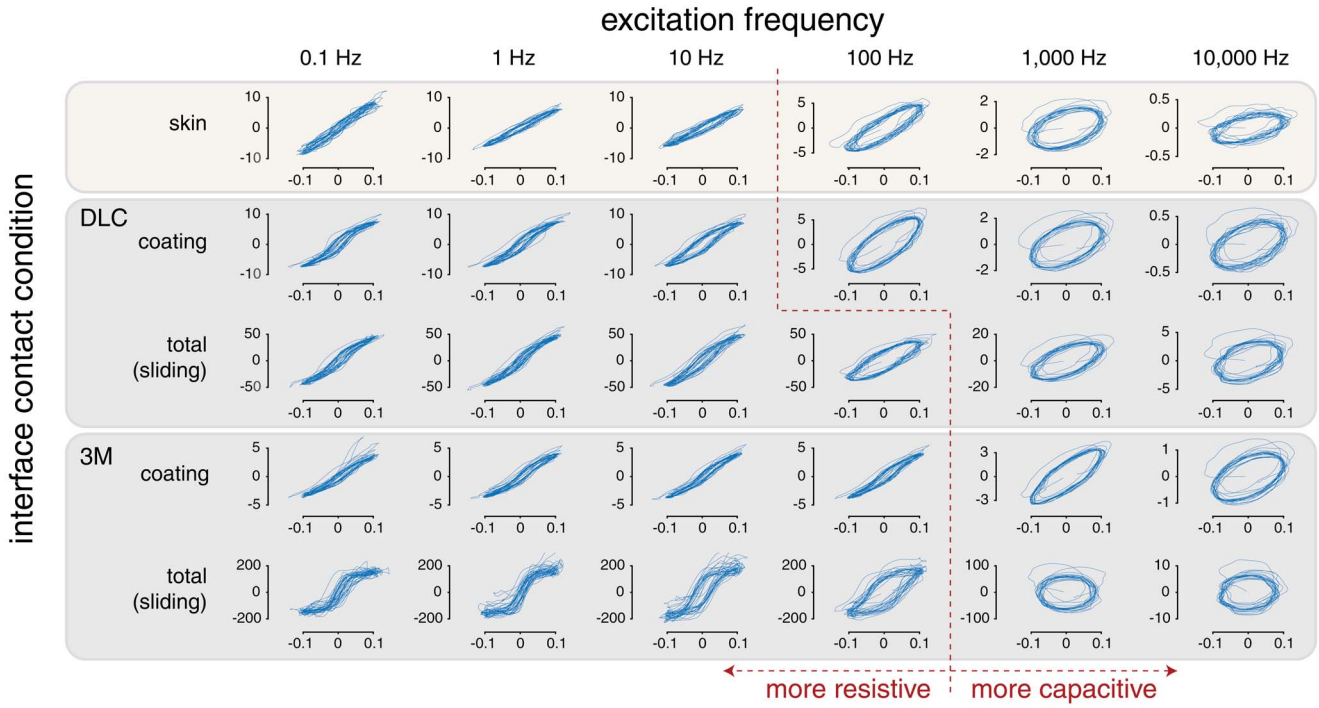

Fig. 6. Set of 30 current vs voltage Lissajous curves (5 interface conditions and 6 frequencies) created using $\pm 0.1mA$ sinusoidal test currents. All horizontal scales are current in milliamps, all vertical scales are voltage in volts.

corner frequencies an order of magnitude above and below the actuation frequency, using zero phase delay butterworth filters. This filtering reduces the effect of noise in the raw data, yet still allows non-linear harmonics to be apparent.

B. Results and Discussion

Data from all 30 experiments (5 conditions, 6 frequencies) are displayed in Fig. 6. There are a number of general trends, and some specific observations to note.

First, all impedances measured appeared to exhibit quasistaic and resistive like behavior at low frequency, and gradually transition into more capacitive like behavior as frequency increased. This is evidenced by the shape of each curve, which moves from an in-phase line like shape at 0.1 Hz, to an out-of-phase ellipse like shape at 10,000 Hz. This transition is also seen in the overall voltage magnitude, which remains approximately constant across each condition for frequencies below 10 Hz, and then attenuates at higher frequencies. The red dashed line in Fig. 6 roughly marks where this transition point takes place for each condition.

Another general trend is that the peak voltage in the (IV) total (sliding) conditions is approximately 2x (for DLC) or 10x (for 3M) the combined peak voltages of the skin and respective coatings. This substantial increase in voltage seen in the (IV) total (sliding) case is the first bit of direct evidence for a large interfacial gap impedance not accounted for by the skin or coating impedances.

In terms of linearity, each condition displayed non-linear behavior in the lower frequency ranges, even for this relatively small $\pm 0.1mA$ current. These effects appear least pronounced in the skin, and more pronounced in each coating. Also, the (IV) total (sliding) case for the 3M screen showed a rapid breakdown type phenomenon at $\approx \pm 150V$, which did not go away until 1,000 Hz, when the resulting voltage fell below this threshold. This breakdown could be heard and felt at the finger in the form of a crackling vibration (but not an electrocutaneous sensation), and is most likely a result of the dielectric breakdown of air in the gap. In contrast to the lower frequencies, linearity at higher frequencies (and currents) appears to be preserved.

The main conclusion from these experiments is that the linearity of the impedance model introduced earlier cannot be taken for granted, and appears only to be valid for small currents, or when the actuation frequency is sufficiently high as to be solely in the capacitive regime.

V. Electrical Impedance Experiments

A. Data Collection

Results from the previous experiment informed the collection of small signal impedance data. All impedances were measured with a 2s $\pm 10\mu A$ sinusoidal test current where all impedances remained linear. The resulting sinusoidal test voltage was recorded, and the complex impedance under test

$$\boldsymbol{Z_{ut}(f)} = \frac{\boldsymbol{V_{out}(f)}}{\boldsymbol{I_{out}(f)}} = |\boldsymbol{Z_{ut}(f)}|e^{j\angle \boldsymbol{Z_{ut}(f)}} \qquad (1)$$

was found using a digital lock-in technique. There were 7 unique impedance curve measurements taken, conditions (I), (III), and (IV) using both coatings, and condition (II) using the skin. Thirty logarithmically spaced frequencies from 1 Hz to 50,000 Hz were tested for each impedance curve measurement (frequency order randomized).

Interface condition (I) was measured at 12 equally spaced locations on the circular path that the finger traverses in condition (III) and (IV), seen Fig. 3. At each location, 4 trials were taken back to back, for a total of 48 impedance curves. A single mean and standard deviation was computed across all trials and locations. Condition (II) was measured at the tip of the lead authors non-dominate index finger with a series of 10 consecutive trials. The finger was wiped with 70% isopropyl alcohol (IPA) solution in-between trials and allowed to dry. Applied normal force was held at approximately 1N with a weight, seen Fig. 4. Similar to condition (I), condition (III) was measured at 12 locations with 4 trials at each location for a total of 48 trials, and a single mean and standard deviation was computed. The finger was cleaned with IPA and allowed to dry before each new location, and at least 10 seconds was allowed to pass between the finger touching the disk and the measurement starting to allow the impedance value to stabilize. Condition (IV) was measured as a series of 10 trials, with the finger and disk cleaned once with IPA at the beginning of all the trials. This was due to the fact that the finger was glued to the FR4 ring, and difficult to remove and clean between trials.

B. Results and Discussion

Results from the electrical impedance measurements are shown in Fig. 7 and Fig. 8. In general, these results are highly consistent with the results from the IV curve experiments, but are able to more quantitatively capture the behavior of the various impedances. The details and interpretation of each measurement are given below:

1) Skin and Body Impedance: Recordings of the skin and body impedance show a small variance from trial to trial, Fig. 7 (top). As seen by the phase angle, the impedance curve can be split into 3 different regimes, a resistive regime at low frequency, a more capacitive regime starting between 10 and 100 Hz, and another resistive regime after 10 kHz.

This impedance behavior is highly consistent with established literature, as, for many in vivo bioimpedance recordings, the stratum corneum dominates the overall impedance at low frequencies (below 10 kHz), while the resistance of the viable layers of skin and underlying tissue dominate at higher frequency [20]. The increase in phase angle and leveling off of the magnitude after 10 kHz, therefore, is due to the internal body impedance between the fingertip and return current electrodes, a fact also confirmed from a 3 electrode measurement near the return current electrodes. It can be modeled as a ideal resistance.

The behavior of the impedance below 10 kHz (due to stratum corneum) cannot be accurately modeled by a pure resistor in parallel with a capacitor, as the overall phase angle never reaches 90°, but levels off just shy of 70°. Instead, it is common to use a constant phase element (CPE) in parallel with a resistive element [20], which we found can reasonably capture the impedance magnitude behavior of our data. Indeed, CPEs are quite common in electrochemical impedance spectroscopy measurements, and can possibly be explained by not a single RC time constant for the impedance,

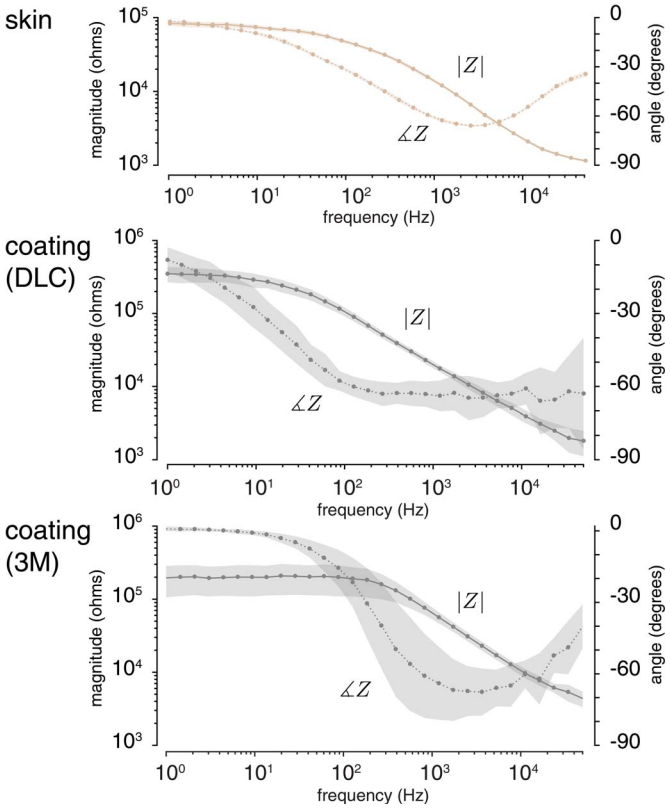

Fig. 7. Skin and body impedance (top), DLC coating impedance (middle), and 3M coating impedance (bottom) as measured in isolation. The centerline represents trial means, while the shaded regions represent $\pm 1\sigma$. A dashed line indicates phase, while a solid line is impedance magnitude. Area of contact $\approx 1cm^2$, and current $= \pm 10\mu A$.

but a distribution of time constants across an interface due to changes in resistivity [21]. In the case of the skin, the parallel resistive behavior is due to the sweat ducts and ionic conduction of the stratum corneum itself, while the capacitive constant phase behavior in this frequency range is most likely due to counterions and other charged (but bound) molecules in the skin interacting with a localized gradient of resistivity increasing from the inner viable skin to the dry and dead outer skin. This interaction could then generate a distribution of RC time constants in the stratum corneum.

2) DLC Coating Impedance: The impedance recorded from the DLC coating, Fig. 7 (middle), shows highly resistive behavior at 1 Hz, which immediately begins a transition to constant phase element like behavior. Consequently, its overall empirical magnitude seems to be captured well by a resistor in parallel with a CPE, but, unlike the skin, not much can be said as to the origin of either the resistive or capacitive effects. The resistive behavior at larger currents is non-ohmic (as seen in Fig 6), therefore some type of semiconductor conduction mechanism is assumed, but analysis beyond this level was not performed, and the there is little in the literature to suggest a specific conduction mechanism. Similarly, the CPE behavior could possibly be caused by a distribution of resistivity within the $2\mu m$ coating, as observed in other thin films [21], interacting with normal polarization mechanisms of the DLC coating.

3) 3M Coating Impedance: The impedance behavior of the 3M coating was unexpected by the authors, as it was previously assumed that the $1\mu m$ silica coating was a pure dielectric insulator, with no low frequency or DC conductivity [14]. As the results of Fig 7 (bottom) show, this is not the case. There is variable resistivity which dominates below approximately 100 Hz. Above 100 Hz, the impedance shows a transition to capacitive behavior and, unlike the skin and DLC coating, it appears to be captured well using an ideal capacitor. This assessment, however, is difficult to make, as, at even higher frequencies, the impedance becomes resistive again, indicating a additional series resistance. Regardless, this coating's overall impedance behavior seems to be captured well using a resistor in series with a resistor and capacitor in parallel.

The physical mechanism for the parallel resistance seen at low frequency is uncertain, though it is believed to be related to a non-conformity (pin-holes) of the coating seen in profilometry data, as SiO_2 typically has a resistivity on the order of 10^{16} Ωm. It could, however, also be due to a semiconductive mechanism. The parallel capacitance is consistent with a typical parallel plate capacitor with the dielectric and geometric properties of the SiO_2, and the series resistance can be explained by the non-zero sheet resistance of the ITO layer.

4) Total Impedance - Sliding and Stopped: Fig. 8 shows the magnitude of total impedance, Z_{total}, measured in both sliding and stopped cases. In the sliding cases, measurements show similar RC characteristics as those in Fig. 7. The 3M case is almost exactly an RC model, while the shallow slope of the DLC case mimics its underlying coating, and can be modeled by a CPE. Compared to the stopped case, however, the sliding data reveal an increase in impedance magnitude of approximately 10x and 2x for the 3M and DLC surfaces respectively. It is unclear why this increase is larger for the 3M screen than the DLC, though its speculated to be caused by the increased surface roughness of the 3M (192nm RMS) coating as compared to the DLC (35nm RMS).

In both cases the total impedance observed while stopped is very nearly equal to the series combination of the respective coating and skin impedances measured in isolation. There is a small difference between the two, however this difference appears consistent with a change in effective contact area between conditions (I)/(II) and condition (IV) (assuming the gross area is in contact with the former, and a smaller area, only the fingerprint ridges, is in contact with the latter).

This fact implies that the large change from the sliding to the stopped case cannot be accounted for by other system impedances, but must be the result of an additional physical impedance mechanism, the so-called gap impedance. To put another way, measurements in Fig. 7 and 8 support the hypothesis that, in going from sliding to stopped, the gap impedance is essentially shorted out, and all that remains is the series combination of the skin and coating impedances. It is hypothesized that this impedance drop is due to a buildup of sweat in the air gap, which is both highly conductive and has a much higher dielectric constant than air, each of which would dramatically lower the gap impedance. However, more evidence is needed to support this claim, as it could also be due to a relaxation of the skin, causing dramatically increased real area of contact, or a combination of effects.

5) Gap Impedance in Relation to the System: With the existence of the interfacial gap impedance in clear view from Fig. 8, we can estimate its value and influence on the to the total system impedance. One way to calculate its value is to simply subtract off the skin and coating impedances from the total impedance seen while sliding:

$$\boldsymbol{Z_{gap} = Z_{total(sliding)} - Z_{skin} - Z_{coating}} \quad (2)$$

With this done, we can also calculate the relative impedance magnitude ratio for the skin, coating and gap impedances. This is defined by

$$ratio = \frac{|\boldsymbol{Z_i}|}{|\boldsymbol{Z_{total(sliding)}}|}, \quad i = skin, coating, gap \quad (3)$$

which allows us to estimate the contribution of each impedance mechanism to the overall system impedance. This ratio is plotted for each element and surface in Fig. 9.

As can be seen, the gap impedance clearly dominates the total impedance seen in the 3M case, and remains a majority of the impedance in the DLC case, across the entire frequency range. This implies that the coating and skin impedances have intrinsically small contributions in relation to the gap, and that, for a given applied voltage or current, only a small voltage drop develop across them. The majority of the voltage will instead develop across the gap.

This is a important point, and one that is most likely true only because the careful selection of the surfaces and

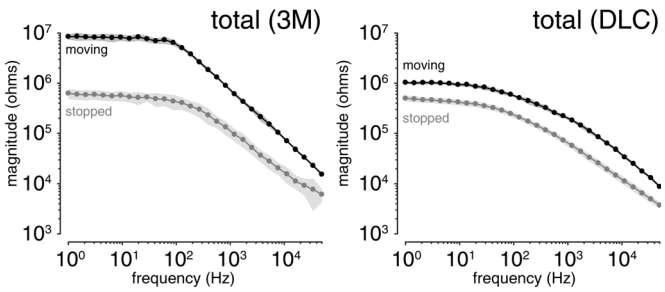

Fig. 8. Measurement of the total system impedance seen while the surface is stopped (III), versus sliding (IV).

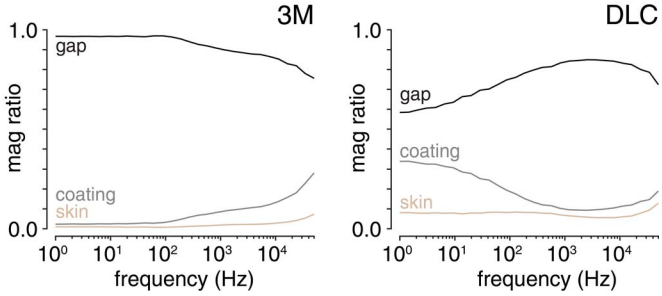

Fig. 9. Calculated magnitude ratio of each given impedance to that of the total systems impedance seen while sliding.

preemptive elimination of other unnecessary impedances. For a thicker dielectric coating, for instance, this will not be the case, nor would it be if the series capacitance of the 3M screen is left intact, or if careful grounding conditions were not ensured. In fact, we propose that the gap impedance magnitude ratio could be viewed going forward as a metric for the electrical effectiveness of an electroadhesive surface given an applied voltage.

VI. Summary and Future Work

We presented a series impedance model based off of empirical measurement techniques and validated the linearity of this approach under certain conditions: small applied currents or high frequencies. The results of these measurements show that the impedance elements can generally be thought of as resistances in parallel with capacitances. However, while the capacitive behavior is ideal for the 3M based measurements, it is not for the skin and DLC based measurements. Both coatings tested can sustain a gap voltage while sliding at all frequencies tested, and therefore can produce both DC and AC electroadhesive forces. The skin and coating impedances appear minimal compared to the gap, implying that future electroadhesive displays should not focus on these layers directly, but should investigate what factors create and influence the gap impedance, as this seems to be a critical electrical system parameter.

The series model behavior employed is verified by the fact that the sum of the impedances measured in conditions (I)/(II) add up to nearly the same impedance seen in condition (III), except for a small difference (consistent with a slight change in effective contact area). Because of this, the difference between $Z_{total(sliding)}$ and $Z_{total(stopped)}$ could also be used to estimate Z_{gap}, as opposed to (2), which might allow for rapid characterization of electroadhesive displays.

Finally, early evidence points to a correlation between interfacial gap impedance and real area of contact seen via FTIR imaging (a technique demonstrated recently by [22] [23]), meaning Z_{gap} could be a good proxy for a measure of real area of contact. If proven, this could be used in future studies to elucidate the nature of fingertip friction, or to estimate area of contact in real-time during usage, expanding the usefulness of the techniques and measurements shown here to a wider research audience.

Acknowledgement

This material is based upon work supported by the National Science Foundation grant number IIS-1518602. Thanks to Oerlikon Balzers Coating USA, Inc. for the DLC coating, and Philip Chehade for processing the 3M discs.

References

[1] E. Gray, "Improvement in electric telegraphs for transmitting musical, tones," U.S. Patent US166 096 A, Jul., 1875, cooperative Classification H04L27/26.

[2] A. Johnsen and K. Rahbek, "A physical phenomenon and its applications to telegraphy, telephony, etc." *Journal of the Institution of Electrical Engineers*, vol. 61, no. 320, pp. 713–725, Jul. 1923.

[3] E. Mallinckrodt, A. L. Hughes, and W. Sleator, "Perception by the Skin of Electrically Induced Vibrations," *Science*, vol. 118, no. 3062, pp. 277–278, 1953.

[4] S. Grimnes, "Electrovibration, cutaneous sensation of microampere current," *Acta Physiologica Scandinavica*, vol. 118, no. 1, pp. 19–25, 1983.

[5] L. D. Hartsough, "Electrostatic wafer holding," *Solid State Technology*, vol. 36, no. 1, pp. 87–91, Jan. 1993.

[6] G. J. Monkman, "An Analysis of Astrictive Prehension," *The International Journal of Robotics Research*, vol. 16, no. 1, pp. 1–10, Feb. 1997. [Online]. Available: http://ijr.sagepub.com/content/16/1/1

[7] H. Prahlad, R. Pelrine, S. Stanford, J. Marlow, and R. Kornbluh, "Electroadhesive robots #x2014;wall climbing robots enabled by a novel, robust, and electrically controllable adhesion technology," in *2008 IEEE International Conference on Robotics and Automation*, May 2008, pp. 3028–3033.

[8] R. M. Strong and D. E. Troxel, "An Electrotactile Display," *IEEE Transactions on Man-Machine Systems*, vol. 11, no. 1, pp. 72–79, Mar. 1970.

[9] D. J. Beebe, C. M. Hymel, K. A. Kaczmarek, and M. E. Tyler, "A polyimide-on-silicon electrostatic fingertip tactile display," in *Proceedings of 17th International Conference of the Engineering in Medicine and Biology Society*, vol. 2, Sep. 1995, pp. 1545–1546 vol.2.

[10] J. Linjama and V. Mkinen, "E-sense screen: Novel haptic display with capacitive electrosensory interface," *HAID*, vol. 9, pp. 10–11, 2009.

[11] O. Bau, I. Poupyrev, A. Israr, and C. Harrison, "TeslaTouch: electrovibration for touch surfaces," in *Proceedings of the 23nd annual ACM symposium on User interface software and technology*, ser. UIST '10. New York, NY, USA: ACM, 2010, pp. 283–292.

[12] D. Meyer, M. Wiertlewski, M. Peshkin, and J. Colgate, "Dynamics of ultrasonic and electrostatic friction modulation for rendering texture on haptic surfaces," in *2014 IEEE Haptics Symposium (HAPTICS)*, Feb. 2014, pp. 63–67.

[13] C. Shultz, E. Colgate, and M. A. Peshkin, "The application of tactile, audible, and ultrasonic forces to human fingertips using broadband electroadhesion," *IEEE Transactions on Haptics*, vol. PP, no. 99, pp. 1–1, 2018.

[14] D. Meyer, M. Peshkin, and J. Colgate, "Fingertip friction modulation due to electrostatic attraction," in *World Haptics Conference (WHC), 2013*, 2013, pp. 43–48.

[15] E. Vezzoli, M. Amberg, F. Giraud, and B. Lemaire-Semail, "Electrovibration Modeling Analysis," in *Haptics: Neuroscience, Devices, Modeling, and Applications*. Springer, Berlin, Heidelberg, Jun. 2014, pp. 369–376.

[16] Y. Vardar, B. Gl, and C. Basdogan, "Effect of Waveform in Haptic Perception of Electrovibration on Touchscreens," in *Haptics: Perception, Devices, Control, and Applications*, Jul. 2016.

[17] J. Kang, H. Kim, S. Choi, K. D. Kim, and J. Ryu, "Investigation on Low Voltage Operation of Electrovibration Display," *IEEE Transactions on Haptics*, vol. 10, no. 3, pp. 371–381, Jul. 2017.

[18] S. Kanno, K. Kato, K. Yoshioka, R. Nishio, and T. Tsubone, "Prediction of clamping pressure in a Johnsen-Rahbek-type electrostatic chuck based on circuit simulation," *Journal of Vacuum Science & Technology B: Microelectronics and Nanometer Structures Processing, Measurement, and Phenomena*, vol. 24, no. 1, pp. 216–223, Jan. 2006. [Online]. Available: http://avs.scitation.org/doi/abs/10.1116/1.2151219

[19] C. Shultz, M. Peshkin, and J. Colgate, "Surface haptics via electroadhesion: Expanding electrovibration with Johnsen and Rahbek," in *2015 IEEE World Haptics Conference (WHC)*, Jun. 2015, pp. 57–62.

[20] S. Grimnes and O. G. Martinsen, *Bioimpedance and Bioelectricity Basics*. Academic Press, Aug. 2014.

[21] B. Hirschorn, M. E. Orazem, B. Tribollet, V. Vivier, I. Frateur, and M. Musiani, "Constant-Phase-Element Behavior Caused by Resistivity Distributions in Films II. Applications," *Journal of The Electrochemical Society*, vol. 157, no. 12, pp. C458–C463, Dec. 2010. [Online]. Available: http://jes.ecsdl.org/content/157/12/C458

[22] M. Wiertlewski, R. F. Friesen, and J. E. Colgate, "Partial squeeze film levitation modulates fingertip friction," *Proceedings of the National Academy of Sciences*, vol. 113, no. 33, pp. 9210–9215, Aug. 2016. [Online]. Available: http://www.pnas.org/content/113/33/9210

[23] S. Bochereau, B. Dzidek, M. Adams, and V. Hayward, "Characterizing and imaging gross and real finger contacts under dynamic loading," *IEEE Transactions on Haptics*, vol. PP, no. 99, pp. 1–1, 2017.